Electronic Supplementary Material (ESI) for Nanoscale Horizons.

Bubbling resilient 3D free-standing nanoporous graphene with encapsulated multicomponent nano-alloy for enhanced electrocatalysis

Linshan Zhu[▽], Qingqing Li[▽], Yixuan Hu[▽], Xin Wu, Kolan Madhav Reddy,* Kaikai Li,* Guoqiang Xie, Xingjun Liu, and Hua-Jun Qiu*

Linshan Zhu, Qingqing Li, Xin Wu, Kaikai Li, Guoqiang Xie, Xingjun Liu, Hua-Jun Qiu

School of Materials Science and Engineering, Harbin Institute of Technology (Shenzhen), Shenzhen, China

E-mail: qiuhuajun@hit.edu.cn; likaikai@hit.edu.cn

Yixuan Hu, Kolan Madhav Reddy

Frontier Research Center for Materials Structure, School of Materials Science and Engineering, Shanghai Jiao Tong University, Shanghai 200240, China

Email: kmreddy@sjtu.edu.cn

Qingqing Li,

Zhejiang Laboratory, Hangzhou 311100, China

Hua-Jun Qiu

Shenzhen Key Laboratory of Advanced Functional Carbon Materials Research and Comprehensive Application, Harbin Institute of Technology, Shenzhen, 518055 China

Experimental

Preparation of nanoporous substrates

$Mn_{70}Ni_{10}Cu_{10}Co_{4.5}Pt_{0.5}$ (at.%) was prepared by melting pure melts (>99.9 wt.%) using an induction melting furnace under the protection of Ar, and then the alloy flake is prepared by cold-rolling to a thickness of ~30 μm at room temperature. The multicomponent nanoporous alloy templates with pore sizes of ~3-5 nm was prepared by chemically dealloying $Mn_{70}Ni_{10}Cu_{10}Co_{4.5}Pt_{0.5}$ (at.%) in a 1.0 M $(NH_4)_2SO_4$ aqueous solution at 50 °C for 12 h. The templates were then washed thoroughly with deionized water and dried in vacuum.

Preparation of nanoporous N-doped graphene/ Pt-based multicomponent alloy

Firstly, the multicomponent nanoporous alloy templates loaded on a corundum plate were inserted into the center of a quartz tube (φ30×φ27×1000 mm) furnace, and subsequently annealed at 800 °C under a mixed atmosphere of Ar (99.99%, 200 sccm) and H_2 (99.99%, 100 sccm) for 3 min as the reduction pre-treatment. Secondly, the N-doped graphene was grown on nanoporous multicomponent alloy ligament surface by introducing pyridine (0.2 mbar, 99.8%, anhydrous, Sigma-Aldrich) vapor with the gas flow of Ar (200 sccm) and H_2 (100 sccm) at 800 °C for 2 min. After that, the furnace was immediately opened, and the inner quartz tube was cooled with a fan to room temperature. The nanoporous N-doped graphene network with encapsulated nanoporous Pt-based multicomponent alloy (NG/PtMnNiCuCo) was finally obtained by etching the CVD-treated sample in 8.0 M HNO_3 for 30 minutes at room temperature

and followed with pure distilled water rinsing for at least three times. In comparison, pure nanoporous N-doped graphene was prepared by using nanoporous Ni as template which was obtained by chemically dealloying $Ni_{30}Mn_{70}$ (at.%) in a 1.0 M $(NH_4)_2SO_4$ aqueous solution at 50 °C. Other fabrication conditions are the same as that of NG/PtMnNiCuCo.

Preparation of virtual seawater

The neutral seawater used for the test was artificially simulated by dissolving 2.686 g NaCl (AR, 99.5%), 0.494 g $MgCl_2 \cdot 8H_2O$ (AR, 98%), 0.705 g $MgSO_4 \cdot 7H_2O$ (AR, 99%), 0.228 g $CaCl_2 \cdot 6H_2O$ (AR, 97%), 0.019 g $NaHCO_3$ (AR, 99.8%), and 0.072 g KCl (AR, 99.5%) in 100 mL of deionized water, and the pH value was detected by the pH detector.

Material characterization

Sample characterization was performed on a JEM-ARM 200F aberration corrected transmission electron microscope (TEM) equipped with energy dispersive X-ray spectrometer (EDS), a HITACHI S-4700 scanning electron microscope (SEM) equipped with EDS, an X-ray diffraction (XRD) diffractometer using Cu Kα radiation (Panalytical aries), and an X-ray photoelectron spectroscopy (XPS, ESCALAB 250). Raman spectra were tested by a Raman microscope (Renishaw in Via-Qontor Raman Microscope) with an incident wavelength of 532 nm.

Electrochemical measurements

All electrochemical measurements were performed on a CHI660E electrochemical workstation with a three-electrode system. The three-electrode system includes a glassy

carbon electrode adhered with a piece of free-standing NG/PtMnNiCuCo with the help of Nafion (2 μL, 0.5 wt %, Aladdin) as working electrode, a carbon rod as the counter electrode, and an Ag/AgCl (filled with saturated KCl solution) as the reference electrode. The following electrochemical tests were performed with a Pt loading of 12 μg Pt cm^{-2}. The scanning rate used in linear scanning voltammetry (LSV) and cyclic voltammetry (CV) is 5 mV s^{-1}. For hydrogen evolution reaction (HER), the solution was 0.5 M H_2SO_4 solution saturated with H_2 (by bubbling pure H_2 for 30 min). For oxygen reduction reaction (ORR), the solution was 0.1 M $HClO_4$ solution saturated with O_2 (by bubbling pure O_2 for 30 min). The current density was normalized to the geometrical area, electrochemical surface area or the mass of noble Pt. The measured potentials vs Ag/AgCl were converted to a reversible hydrogen electrode (RHE) scale according to the Nernst equation ($E_{RHE} = E_{Ag/AgCl} + 0.0592\ pH + 0.197$).

The electron transfer number (n) during ORR was estimated by measuring the diffusion-limiting current density (j_L) at different rotating speed (ω) of the working electrode according to Koutecky-Levich equations (1):

$$\frac{1}{j} = \frac{1}{j_L} + \frac{1}{j_K} = \frac{1}{B\omega^{-\frac{1}{2}}} + \frac{1}{j_K} = \frac{1}{(0.2nFC_0D_0^{2/3}\nu^{-1/6})\omega^{1/2}} + \frac{1}{j_K} \quad (1)$$

where F is the Faraday constant (96485 C mol^{-1}); C_0 and D_0 are the bulk concentration (1.2×10^{-6} mol cm^{-3}) and diffusion coefficient (1.9×10^{-5} cm^2 s^{-1}) of O_2 in 0.1 M $HClO_4$, respectively; υ is the kinematic viscosity of the electrolyte (0.01 cm^2 s^{-1}).

DFT calculations

The DFT calculations were performed using the Vienna ab initio Simulation Package

(VASP). Perdew, Burke, and Ernzerhof (PBE) functional of generalized gradient approximation (GGA) with projector augmented wave (PAW) was applied to describe the electronic structures of materials. The plane-wave-basis kinetic energy cutoff was set to 400 eV. The Brillouin zones are sampled using Gamma-centered k-mesh of 3 × 3 × 1. The vacuum layers are set to ~15Å to decouple the interaction between periodic images. The rest atomic layers and adsorbates are free to relax until the net force per atom is less than 0.05 eV/Å.

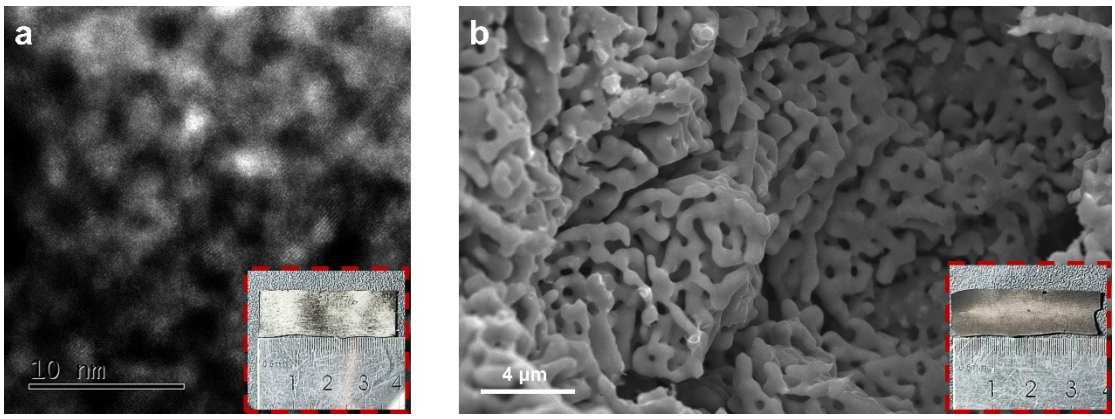

Figure S1. (a) HAADF-STEM image and photograph (inset in a) of the nanoporous MnNiCuCoPt template obtained by dealloying. (b) SEM image and photograph (inset in b) of nanoporous template after CVD growth of graphene.

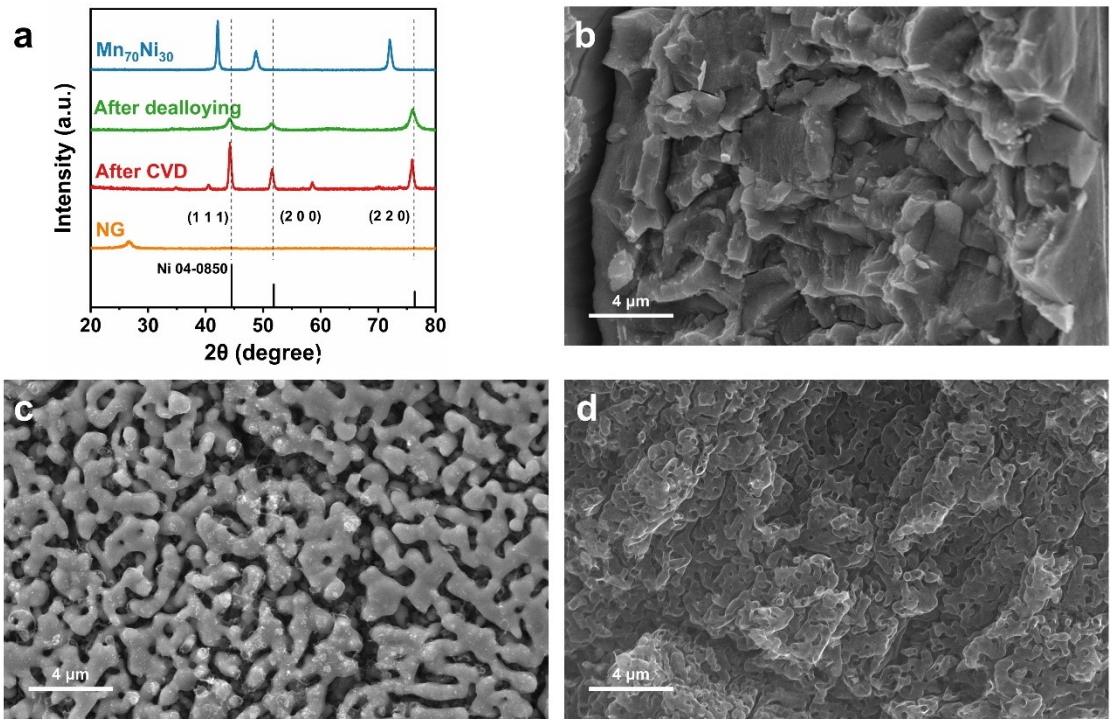

Figure S2. (a) XRD patterns of the precursor NiMn alloy, dealloyed nanoporous Ni, after CVD growth of graphene and after the removal of the templates by HNO_3 (i.e., NG). SEM images of the (b) obtained nanoporous Ni, (c) the coarsened nanoporous Ni after CVD growth of graphene and (c) the nanoporous N-doped graphene (NG) after the removal of porous Ni template.

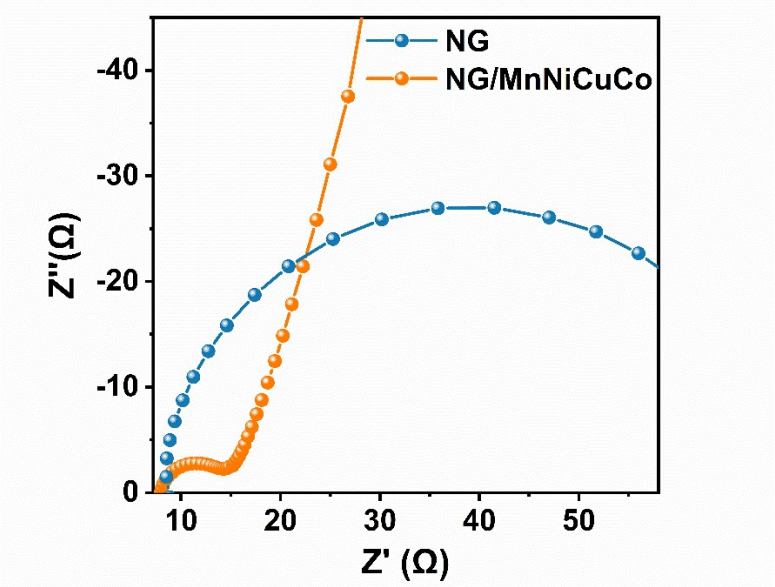

Figure S3. Electrochemical impedance spectroscopy (EIS) collected in the frequency range of 0.01–10^5 Hz.

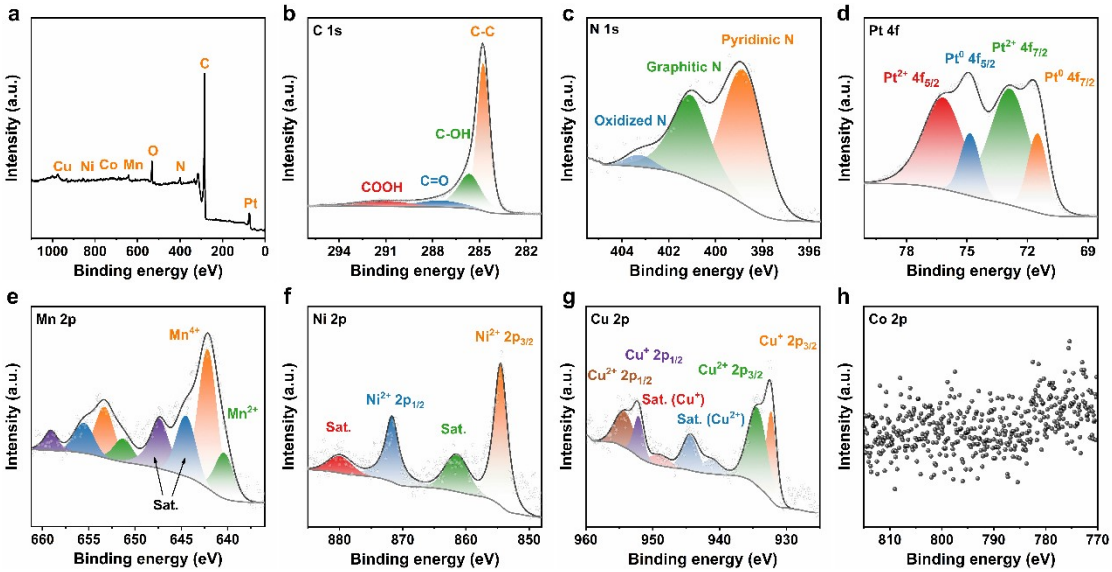

Figure S4. XPS spectra of nanoporous composite: (a) full XPS survey, (b) C 1s, (c) N 1s, (d) Pt 4f, (e) Mn 2p, (f) Ni 2p, (g) Cu 2p, (h) Co 2p.

In Figure S4, Ni are mainly in the states of Ni^{2+}. High resolution XPS region scan of Mn 2p reveals the existence of both Mn^{2+} and Mn^{4+} (*Angew. Chem. Int. Ed.*, 2023, 62, 202302329). The Cu 2p spectrum suggests the presence of both Cu^{+} and Cu^{2+} on the nanoporous alloy surface. Cobalt has

been etched to a very low level on the surface. Considering the detected Co by STEM-EDS, it is reasonable to believe that most residual Co are inside of the nanoalloy. The Pt 4f spectrum shows that Pt are in the form of both Pt^0 and Pt^{2+} (Figure S4). Compared with that of nanoporous PtCu alloy dealloyed in the same 8 M HNO_3 solution (*ACS Catal.* **2015**, *5* (6), 3779–3785), the ratio of Pt^{2+} in the dealloyed multicomponent Pt alloy is much higher ($Pt^{2+}/Pt^0 \approx 3$), which may be due to the presence of many single atoms (as shown in Figure 2f). Because the zero-valent metal single atoms are extremely unstable, it needs to form a chemical bond with oxygen or nitrogen to keep stable. The presence of single atom-based noble metals can be helpful for many catalytic reactions (*J. Am. Chem. Soc.* **2022**, *144* (40), 18155–18174).

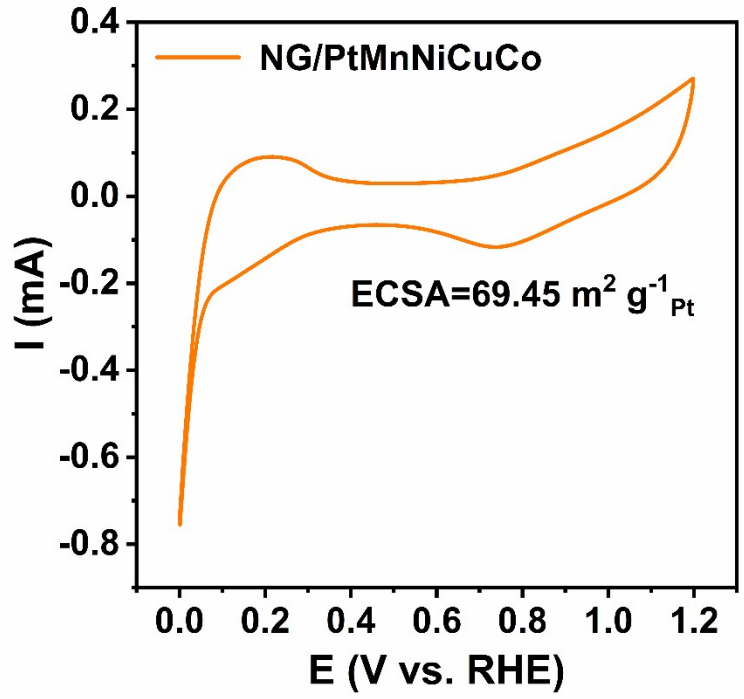

Figure S5. CV curves of the 3D graphene/nanoporous alloy composite recorded in N_2 saturated 0.1 M $HClO_4$ solution at a sweep rate of 50 mV s^{-1}.

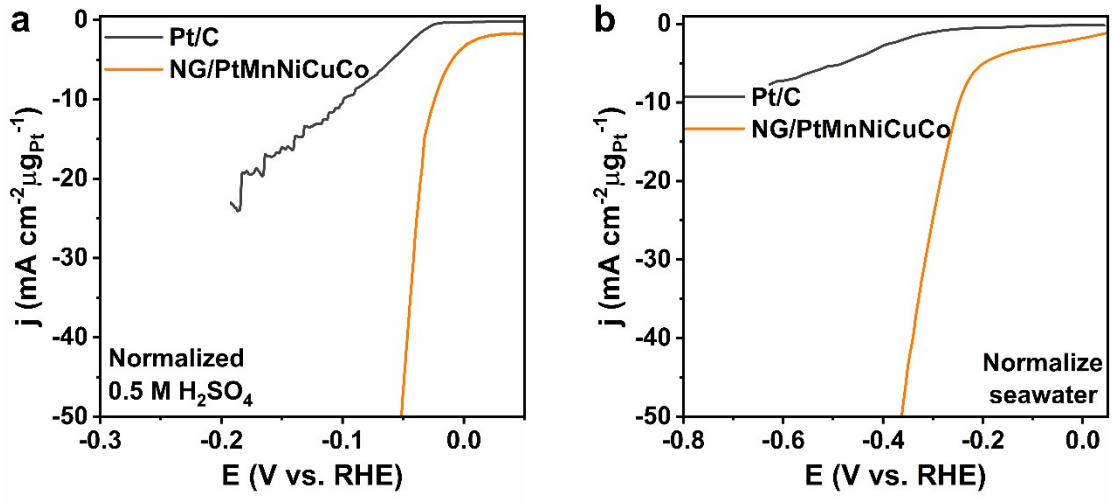

Figure S6. (a) LSV curves in the 0.5 M H_2SO_4 normalized by loaded Pt on electrodes. (b) LSV curves in the seawater normalized by Pt loading amounts on electrodes.

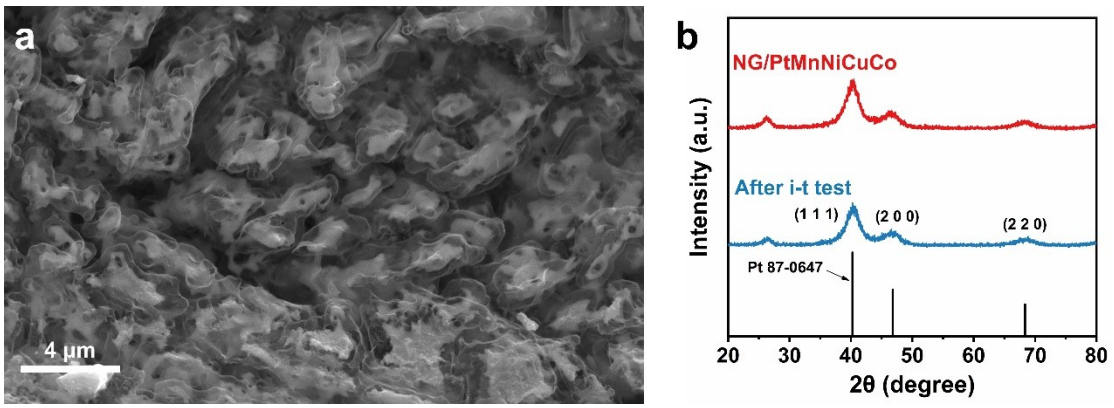

Figure S7. (a) SEM image of the NG/PtMnNiCuCo after i-t test in 0.5 M H_2SO_4. (b) XRD of the NG/PtMnNiCuCo before and after i-t test in 0.5 M H_2SO_4.

Table S1. The atomic percentages of Mn, Ni, Cu, Co, and Pt in different stages of the sample were measured from SEM-EDS.

Sample	Content (at.%)				
	Mn	Ni	Cu	Co	Pt
precursor	74.64	10.45	10.13	4.31	0.47
After dealloying	11.96	34.81	35.32	16.95	0.96
After CVD	11.04	35.21	35.52	17.25	0.98
NG/PtMnNiCuCo	8.37	13.15	14.28	12.83	51.37
After i-t test	7.81	14.13	13.98	11.91	52.71

Table S2. Content of metal elements in NG/PtMnNiCuCo from STEM-EDS.

Element	Content (at.%)
Pt	57
Mn	9
Ni	17
Co	17

Due to the interference of Cu grid, the Cu content is ignored.

Table S3. Comparison of the ORR activity of NG/PtMnNiCuCo with various recently reported Pt-based catalysts in acidic media.

Catalysts	Half-wave potential (V vs. RHE)	Tafel slope (mV dec^{-1})	Pt loading (ugPt cm^{-2})	Ref.
NG/PtMnNiCuCo	0.90	60.4	12	This work
PtA@Fe_{SA}-N-C	0.923	64	13	1
PtCu NSs/C	0.893	79.2	18.9	2
$PtCo_3$-H600	0.905	----	12	3
Pt_1Co_{100}/N-GCNT	0.85	82	----	4
Pd@PtCu	0.89	----	15	5
4% Ga−Pt_3Co	0.894	----	36.7	6
$PtNi_3$@OMC-A	0.907	----	15.3	7
PtBi/C	0.886	----	10	8
Pt/CNTs	0.85	----	20	9
Pt-Ni@Pt_D/G	0.83	70	20	10
Pt@Mn-SAs/N-C	0.896	----	7.92	11
Pt-SnS2/SnO_2-90	0.895	----	18.7	12
Pt/NHPC-800	0.878	----	18.65	13
Pt-C-N	0.84	71.4	0.54	14
Pt-PANI	0.878	----	28	15
PtRhNiFeCu/C	0.9	----	10.2	16
PtCuGaFeCo NPs	0.88	55	----	17
Pt_4FeCoCuNi/C	0.943	51.5	8.57	18
Pt/TiC@TiO_2-C	0.84	77	----	19
PFCNC-HEA	0.88	68	----	20

Table S4. Comparison of the HER activity of NG/PtMnNiCuCo with various recently reported Pt-based catalysts in acidic media.

Catalysts	Overpotential @10mA cm^{-2} (mV)	Tafel slope ($mV\ dec^{-1}$)	Pt loading ($ugPt\ cm^{-2}$)	Ref.
NG/PtMnNiCuCo	23	26.4	12	This work
Pt_2Sr/NC	27	26	18.64	21
Pt-$W_{18}O_{49}$	23	30	20.5	22
Pt@Co SAs-ZIF-NC	27	21	14	23
Pt Cs/MoO_2 NSs-L	47	36	----	24
Pt_2Co_8@N-C	47	48	200	25
PtRh DNAs	27	40	----	26
Pt_3Fe/BNC	38	31.3	----	27
Pt–V_2CT_x	27	36.5	14	28
Pt/Mxene	34	29.7	----	29
Pt/CoO_x-HCS-3000	28	31	----	30
Pt_3Fe/NMCS-A	13	21	408	31
5% 1T-PtO_2/C	12	18.6	4.7	32
m-Pt@MoS_2	47	32	12.9	33
$Pt_{0.04}$/Ni-DA	18	34.32	17.7	34
Pt@PtIr NDs	22	14.6	15.48	35
$Au_{81}Pd_2Pt_9$-$S^{B4.6A3.4}_{8}$	35	14.4	----	36
2.5 mM Pt-HEC	70	47	----	37
Pt-Er/h-NC	25	17.1	7.07	38
5%Pt-Ru ONAs/C	31	32.4	----	39
Pt/CoO_x-HCS-3000	28	31	----	40

Reference

1 X. Ao, W. Zhang, B. Zhao, Y. Ding, G. Nam, L. Soule, A. Abdelhafiz, C. Wang and M. Liu, *Energy Environ. Sci.*, 2020, **13**, 3032–3040.

2 W. Li, Z.-Y. Hu, Z. Zhang, P. Wei, J. Zhang, Z. Pu, J. Zhu, D. He, S. Mu and G. Van Tendeloo, *J. Catal.*, 2019, **375**, 164–170.

3 Z. Wang, X. Yao, Y. Kang, L. Miao, D. Xia and L. Gan, *Adv. Funct. Mater.*, 2019, **29**, 1902987.

4 X. Cheng, Y. Wang, Y. Lu, L. Zheng, S. Sun, H. Li, G. Chen and J. Zhang, *Appl. Catal. B*, 2022, **306**, 121112.

5 M. Bao, I. S. Amiinu, T. Peng, W. Li, S. Liu, Z. Wang, Z. Pu, D. He, Y. Xiong and S. Mu, *ACS Energy Lett.*, 2018, **3**, 940–945.

6 M. Li, Z. Zhao, Z. Xia, Y. Yang, M. Luo, Y. Huang, Y. Sun, Y. Chao, W. Yang, W. Yang, Y. Yu, G. Lu and S. Guo, *ACS Catal.*, 2020, **10**, 3018–3026.

7 K. Wang, Y. Wang, S. Geng, Y. Wang and S. Song, *Adv. Funct. Mater.*, 2022, **32**, 2113399.

8 Y. Qin, M. Luo, Y. Sun, C. Li, B. Huang, Y. Yang, Y. Li, L. Wang and S. Guo, *ACS Catal.*, 2018, **8**, 5581–5590.

9 X. Tong, J. Zhang, G. Zhang, Q. Wei, R. Chenitz, J. P. Claverie and S. Sun, *Chem. Mater.*, 2017, **29**, 9579–9587.

10 X. Lyu, Y. Jia, X. Mao, D. Li, G. Li, L. Zhuang, X. Wang, D. Yang, Q. Wang, A. Du and X. Yao, *Adv. Mater.*, 2020, **32**, 2003493.

11 L. Gong, J. Zhu, F. Xia, Y. Zhang, W. Shi, L. Chen, J. Yu, J. Wu and S. Mu, *ACS Catal.*, 2023, **13**, 4012–4020.

12 Z. Lin, J. Liu, S. Li, J. Liang, X. Liu, L. Xie, G. Lu, J. Han, Y. Huang and Q. Li, *Adv. Funct. Mater.*, 2023, **33**, 2211638.

13 M. Li, F. Liu, S. Pei, Z. Zhou, K. Niu, J. Wu and Y. Zhang, *Nanomaterials*, 2023, **13**, 444.

14 L. Zhang, T. Li, T. Du, X. Dai, L. Zhang, C. Tao, J. Ding, C. Yan and T. Qian, *Inorg. Chem.*, 2024, **63**, 2138–2147.

15 S. Xue, R. Yang, C. Lei, J. Zhao, S. Sun, M. Zhao, Z. Wang, Q. Huang and Y. Wu, *Chem. Eng. J.*, 2024, **485**, 149891.

16 Z. Hu, K. Chen, Y. Zhu, B. Liu and J. Shen, *Small*, 2024, 2309819.

17 H. Kuang, Z. Xu, X. Tan, K. Yu and C. Chen, *Small*, 2024, 2308421.

18 Y. Wang, N. Gong, H. Liu, W. Ma, K. Hippalgaonkar, Z. Liu and Y. Huang, *Adv. Mater.*, 2023, **35**, 2302067.

19 C. Zheng, X. Sun, Y. Qin, J. Li, G. Jin, X. Tong and N. Yang, *Adv. Sustainable Syst.*, 2024, **8**, 2300556.

20 T. Chen, F. Ning, J. Qi, G. Feng, Y. Wang, J. Song, T. Yang, X. Liu, L. Chen and D. Xia, *iScience*, 2023, **26**, 105890.

21 X. Liu, S. Hao, G. Zheng, Z. Su, Y. Wang, Q. Wang, L. Lei, Y. He and X. Zhang, *J. Energy Chem.*, 2022, **64**, 315–322.

22 W. X. Li, Z. Y. Liu, S. C. Yang, J. N. Wu, L. Sun, E. G. Ma, H. G. Yang and X. Guo, *Sci. China Mater.*, 2022, **65**, 3435–3441.

23 L. Liang, H. Jin, H. Zhou, B. Liu, C. Hu, D. Chen, Z. Wang, Z. Hu, Y. Zhao, H.-W. Li, D.

He and S. Mu, *Nano Energy*, 2021, **88**, 106221.
24 X. Li, J. Yu, J. Jia, A. Wang, L. Zhao, T. Xiong, H. Liu and W. Zhou, *Nano Energy*, 2019, **62**, 127–135.
25 W. Ren, W. Zang, H. Zhang, J. Bian, Z. Chen, C. Guan and C. Cheng, *Carbon*, 2019, **142**, 206–216.
26 Z. Han, R.-L. Zhang, J.-J. Duan, A.-J. Wang, Q.-L. Zhang, H. Huang and J.-J. Feng, *Int. J. Hydrogen Energy*, 2020, **45**, 6110–6119.
27 Y. Qiao, J. Cui, F. Qian, X. Xue, X. Zhang, H. Zhang, W. Liu, X. Li and Q. Chen, *ACS Appl. Nano Mater.*, 2022, **5**, 318–325.
28 S. Park, Y.-L. Lee, Y. Yoon, S. Y. Park, S. Yim, W. Song, S. Myung, K.-S. Lee, H. Chang, S. S. Lee and K.-S. An, *Appl. Catal. B*, 2022, **304**, 120989.
29 Y. Wu, W. Wei, R. Yu, L. Xia, X. Hong, J. Zhu, J. Li, L. Lv, W. Chen, Y. Zhao, L. Zhou and L. Mai, *Adv. Funct. Mater.*, 2022, **32**, 2110910.
30 Y. Wang, B. Zhu, B. Cheng, W. Macyk, P. Kuang and J. Yu, *Appl. Catal. B*, 2022, **314**, 121503.
31 P. Kuang, Z. Ni, B. Zhu, Y. Lin and J. Yu, *Adv. Mater.*, 2023, **35**, 2303030.
32 H. Yang, Y. Ji, Q. Shao, W. Zhu, M. Fang, M. Ma, F. Liao, H. Huang, Y. Zhang, J. Yang, Z. Fan, Y. Li, Y. Liu, M. Shao and Z. Kang, *Energy Environ. Sci.*, 2023, **16**, 574–583.
33 J. Wang, W. Zang, X. Liu, J. Sun, S. Xi, W. Liu, Z. Kou, L. Shen and J. Wang, *Small*, 2024, 2309427.
34 Y. Peng, K. Ma, T. Xie, J. Du, L. Zheng, F. Zhang, X. Fan, W. Peng, J. Ji and Y. Li, *ACS Appl. Mater. Interfaces*, 2023, **15**, 27089–27098.
35 C. Liu, Z. Wei, M. Cao and R. Cao, *Nano Res.*, 2024, **17**, 4844–4849.
36 Y. Fan, X. Zhang, M. Zhang, X. Yue, W. Du and H. Xia, *Chem. Eng. J.*, 2023, **470**, 144149.
37 D. Kim, S. Surendran, Y. Jeong, Y. Lim, S. Im, S. Park, J. Y. Kim, S. Kim, T. Kim, B. Koo, K. Jin and U. Sim, *Adv. Mater. Technol.*, 2023, **8**, 2200882.
38 G. Chen, W. Chen, R. Lu, C. Ma, Z. Zhang, Z. Huang, J. Weng, Z. Wang, Y. Han and W. Huang, *J. Am. Chem. Soc.*, 2023, **145**, 22069–22078.
39 Q. Yao, J. Le, S. Yang, J. Cheng, Q. Shao and X. Huang, *Chinese Journal of Catalysis*, 2022, **43**, 1493–1501.
40 Y. Wang, B. Zhu, B. Cheng, W. Macyk, P. Kuang and J. Yu, *Applied Catalysis B: Environmental*, 2022, **314**, 121503.